IOP Publishing Journal of Physics G: Nuclear and Particle Physics
J. Phys. G: Nucl. Part. Phys. **44** (2017) 044002 (14pp) https://doi.org/10.1088/1361-6471/aa5ae7

Neutron-capture rates for explosive nucleosynthesis: the case of ^{68}Ni(n, γ)^{69}Ni

A Spyrou[1,2,3,10], A C Larsen[4], S N Liddick[1,3,5], F Naqvi[1,3], B P Crider[1], A C Dombos[1,2,3], M Guttormsen[4], D L Bleuel[6], A Couture[7], L Crespo Campo[4], R Lewis[1,5], S Mosby[7], M R Mumpower[7], G Perdikakis[1,3,8], C J Prokop[1,5], S J Quinn[1,2,3], T Renstrøm[4], S Siem[4] and R Surman[9]

[1] National Superconducting Cyclotron Laboratory, Michigan State University, East Lansing, MI 48824, United States of America
[2] Department of Physics & Astronomy, Michigan State University, East Lansing, MI 48824, United States of America
[3] Joint Institute for Nuclear Astrophysics, Michigan State University, East Lansing, MI 48824, United States of America
[4] Department of Physics, University of Oslo, NO-0316 Oslo, Norway
[5] Department of Chemistry, Michigan State University, East Lansing, MI 48824, United States of America
[6] Lawrence Livermore National Laboratory, 7000 East Avenue, Livermore, CA 94550-9234, United States of America
[7] Los Alamos National Laboratory, Los Alamos, NM, 87545, United States of America
[8] Department of Physics, Central Michigan University, Mt. Pleasant, MI, 48859, United States of America
[9] Department of Physics, University of Notre Dame, Notre Dame, IN 46556, United States of America

E-mail: spyrou@nscl.msu.edu

Received 29 September 2016, revised 6 January 2017
Accepted for publication 20 January 2017
Published 22 February 2017

Abstract

Neutron-capture reactions play an important role in heavy element nucleosynthesis, since they are the driving force for the two processes that create the vast majority of the heavy elements. When a neutron capture occurs on a short-lived nucleus, it is extremely challenging to study the reaction directly and therefore the use of indirect techniques is essential. The present work reports on such an indirect measurement that provides strong constraints on the ^{68}Ni(n, γ)^{69}Ni reaction rate. This is done by populating the compound

[10] This article belongs to the special issue: Emerging Leaders which features invited work from the best early-career researchers working within the scope of *J Phys G*. This project is part of the *Journal of Physics* series' 50th anniversary celebrations in 2017. Artemis Spyrou was selected by the Editorial Board of *J Phys G* as an Emerging Leader.

nucleus ^{69}Ni via the β decay of ^{69}Co and measuring the γ-ray deexcitation of excited states in ^{69}Ni. The β-Oslo method was used to extract the γ-ray strength function and the nuclear level density. In addition the half-life of ^{69}Co was extracted and found to be in agreement with previous literature values. Before the present results, the ^{68}Ni(n, γ)^{69}Ni reaction was unconstrained and the purely theoretical reaction rate was highly uncertain. The new uncertainty on the reaction rate based on the present experiment (variation between upper and lower limit) is approximately a factor of 3. The commonly used reaction libraries JINA-REACLIB and BRUSLIB are in relatively good agreement with the experimental rate. The impact of the new rate on weak *r*-process calculations is discussed.

Keywords: nuclear astrophysics, *r* process, nucleosynthesis, neutron-capture reactions, nuclear level density, γ-ray strength function

(Some figures may appear in colour only in the online journal)

1. Introduction

The creation of elements in the Universe is one of the major open questions of our time. Multiple fields of science come together and provide different pieces to the nucleosynthesis puzzle. Astronomical observations, meteoritic analysis, astrophysical simulations, nuclear structure and reactions calculations, and experimental nuclear data are all paramount for the better understanding of these complex astrophysical processes. Since the original publications of a comprehensive picture of stellar nucleosynthesis 60 years ago [1, 2], the field has evolved and expanded. Many questions have certainly been answered, however many still remain, and new ones have been formulated. New techniques and new tools are developed constantly, each of which opens a new window into our understanding of the Universe. For example, the recent observation of gravitational waves is such a 'window', with great potential to enrich our knowledge of compact objects during merging events [3].

One particularly challenging piece of the stellar nucleosynthesis puzzle is the origin of the heavy elements (heavier than Fe). Three processes are considered responsible for creating the bulk of the isotopes of these elements: the slow neutron capture process (*s* process) [4], the rapid neutron capture process (*r* process) [5, 6], and the *p* process [7, 8], which is responsible for producing the small fraction of neutron-deficient isotopes. The two neutron-induced processes dominate the isotope production, with the *s* process occurring over longer time scales ($\sim 10^3$ yr) and progressing along the valley of stability, and the *r* process extending far into exotic neutron-rich nuclei during extremely short time scales ($\sim$1 s). The explosive nature of the *r* process and the fact that the nuclei involved are very neutron-rich and largely inaccessible for experiments at current facilities, are two of the many reasons that keep the *r* process at the center of attention, despite six decades of study.

The astrophysical site where the *r* process occurs has not been unambiguously determined. Many scenarios have been proposed over the years (e.g. reviews [5, 6]), with the most dominant so far being the core-collapse supernovae, e.g. [9–12], and the neutron-star merger, e.g. [13–15], scenarios. The latter scenario has recently gained even more interest because of the possibility of a 'kilonova' afterglow coming from the decaying *r*-process elements [16]. Recent observations of dwarf spheroidal galaxies [17] showed that the observed patterns are consistent with an *r* process taking place in rare events, consistent with the neutron-star

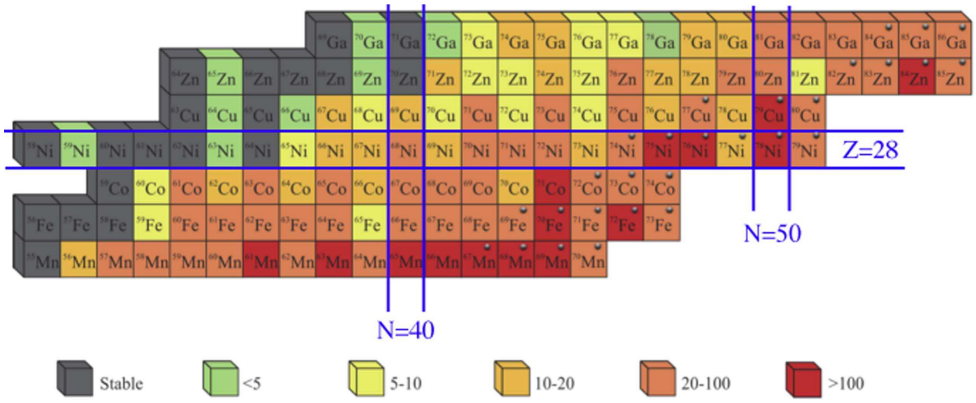

Figure 1. Theoretical neutron-capture reaction rate variations (ratio between maximum and minimum rates) around mass 70. The nucleus in each box represents the target nucleus. The black dots indicate nuclei which do not have a known mass listed in AME2012 [28]. Figure adapted with permisson from [29]. Copyright 2016 by the American Physical Society. See text for details.

merger scenario but not exclusively. In addition, there is the possibility for contributions from more than one astrophysical scenario. In such a case, heavy elements ($A > 120$) are considered to be produced in a 'main' *r* process, while the lighter elements with $A \approx 80$–120 may have strong additional contributions or even a distinct origin ('weak' *r* process). It is therefore clear that the study of the *r* process is a very lively field with a continuous flow of improved astrophysical scenarios and new observational information.

On top of the large effort to understand the uncertainties associated with the astrophysical conditions, it is extremely important to provide accurate nuclear physics input. Sensitivity studies show that the *r*-process abundance distribution changes significantly when varying the nuclear physics input within uncertainties (e.g. most recently [18–20] and references therein). The properties that influence the *r*-process flow and the final abundance distribution are nuclear masses, β-decay rates, β-delayed neutron emission probabilities, and neutron-capture reaction rates. Experiments have provided significant information for masses and β-decay properties, and new experiments are being planned at current and future facilities. However, neutron-capture reaction rate measurements have been extremely challenging experimentally due to the fact that neither of the two reactants (neutron and short-lived, neutron-rich nucleus) can be developed as a target for accelerator based measurements. For this reason the development of indirect techniques that will provide experimental constraints on these important reactions is critical. Several techniques have been developed or are currently under development, such as the surrogate reaction technique [21–23], the γ-ray strength function method [24], and the Oslo method [25, 26]. These techniques are all reaction-based, and as such, they require a relatively high beam intensity to be applied. An alternative technique, the β-Oslo method, was proposed recently, which is a combination of the traditional Oslo method with β decay and total absorption spectroscopy techniques [27]. This latter technique is the focus of the present work, applied for the first time to the β decay of ^{69}Co, populating ^{69}Ni and extracting the reaction rate of the ^{68}Ni(n, γ)^{69}Ni reaction. This reaction has been identified in a weak *r*-process sensitivity study [18] as one of the reactions that influences the final abundance distribution.

Table 1. Nuclear level density and γ-ray strength function models used as input in the TALYS calculations presented in figure 1.

Nuclear level density models	TALYS-1.6 *ldmodel*	Reference
Constant temperature matched to the Fermi gas model (CT + BSFG)	1	[35]
Back-shifted Fermi gas model (BSFG)	2	[35, 36]
Generalized super fluid model (GSM)	3	[37, 38]
Hartree–Fock using Skyrme force (HFS)	4	[39]
Hartree–Fock–Bogoliubov (Skyrme force) + combinatorial method (HFBS—C)	5	[40]
γ-ray Strength Function models	**TALYS-1.6 *strength***	**Reference**
Kopecky–Uhl generalized Lorentzian (KU)	1	[41]
Hartree–Fock BCS + QRPA (HF-BCS + QRPA)	3	[42]
Hartree–Fock–Bogoliubov + QRPA (HFB + QRPA)	4	[43]
Modified Lorentzian (Gor-ML)	5	[44]

Figure 1 shows a fraction of the chart of nuclei around the region of interest. The color code represents the variation in the predicted reaction rate using the code TALYS-1.6 [30] with different nuclear reaction input parameters (ratio between maximum and minimum rate at 1.5 GK). Specifically, a compound nucleus neutron-capture reaction cross section is calculated using the relevant nuclear masses, the neutron-nucleus optical model potential (nOMP), the nuclear level density (NLD), and the γ-ray strength function (γSF). For the nuclei shown in figure 1, the majority of the masses are known experimentally and are listed in the Atomic Mass Evaluation 2012 (AME2012) [28]. Nuclei marked with a black dot, do not have a mass listed in AME2012, or their mass is the result of an extrapolation. The neutron-capture reaction rate calculations seem to change with the nOMP variation only mildly [31]. Therefore, the two parameters that dominate the uncertainties in the reaction rates are the NLD and the γSF. These are the two quantities that were varied to create figure 1. Table 1 presents a list of the NLD and γSF models used in these calculations. For the reasons discussed in [29], out of the six available NLD models in TALYS-1.6, the temperature-dependent Hartree–Fock–Bogoliubov level densities using the Gogny force based on Hilaire's combinatorial tables [32] was excluded (*ldmodel 6*), and out of the five γSF models, the Brink–Axel single Lorentzian formula [33, 34] was also excluded (*strength 2*).

Figure 1 shows that the calculations diverge as one moves farther from the last stable isotope. While the variation between models is less than a factor of 5 around stability, already the addition of two neutrons (e.g. Mn, Fe and Co chains) results in over a factor of 20 difference between models. In particular, for the reaction of interest for the present work, ^{68}Ni $(n, \gamma)^{69}$Ni, the calculations exhibit a variation in the theoretical calculations of a factor 35. In the present work we report on the first experimental constraint for this reaction. We use the β-Oslo method to extract the NLD and γSF for the compound nucleus ^{69}Ni. These two experimental quantities are used as input in the TALYS calculations to provide an experimentally constrained reaction rate. The experimental results are also used in weak *r*-process calculations to show the impact on the final abundance distribution.

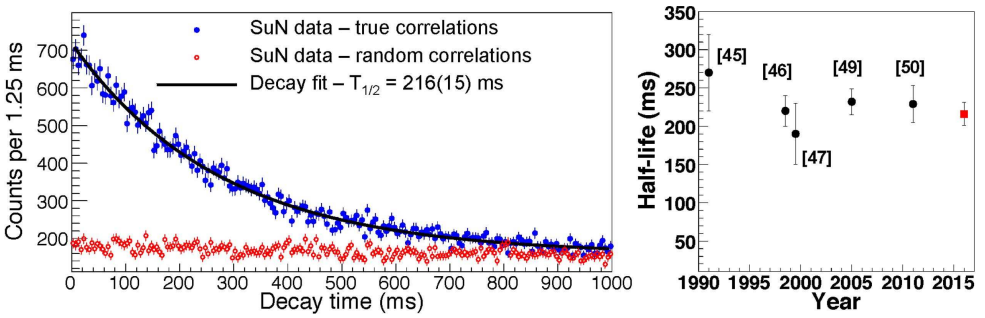

Figure 2. ^{69}Co half-life extraction. The left-hand figure shows the experimental data in the blue, filled dots and the best fit in the solid line. The red, open circles show the random correlation background. The resulting half-life of 216(15) ms is shown in the right-hand figure as a red square, compared with black points that correspond to the literature values from Bernas *et al* (1991), Mueller *et al* (1999), Sorlin *et al* (1999), Gaudefroy (2005), and Daugas *et al* (2011) [46–50].

2. Methods

The experiment took place at the National Superconducting Cyclotron Laboratory, at Michigan State University. A ^{86}Kr primary beam was accelerated to 140 MeV nucleon^{-1} at the Coupled Cyclotron Facility, and was impinged on a Be production target. The A1900 fragment separator [45] was used to select the isotope of interest ^{69}Co as part of a 'cocktail' consisting of approximately twelve isotopes in this mass region [29]. ^{69}Co was identified event-by-event based on energy loss and time-of-flight information from a plastic scintillator at the focal plane of the A1900, and two Si PIN detectors upstream of the implantation point. The beam ions were implanted in a 1 mm thick double sided silicon strip detector (DSSD), consisting of two sets of sixteen strips, perpendicular to each other, 1.2 mm apart. The signal from the DSSD was fed into dual gain preamplifiers, which provided information about implanted ions (low gain) and the emitted β-decay electrons (high gain). Downstream of the DSSD, a 0.5 mm thick Si detector was used to 'veto' any unwanted light ions that were part of the beam cocktail. The β and ion information were correlated in space and time, in order to assign the detected β particles to the appropriate ion. This technique is not free of background, and for this reason random correlations were also created by identifying events where β particles and ions were not correlated in space.

The correlation time between ion implantation and β detection was used to confirm the previously known half-life of ^{69}Co, as shown in figure 2. The best fit to the data is represented by the solid line and it included the exponential decay curve as well as the random background. The extracted half-life of 216(15) ms is in excellent agreement with previous measurements [46–48, 50, 51]. The half-life of the daughter nucleus (^{69}Ni) is more than a factor of 10 longer than the ^{69}Co one (ground state 11.2 s, 321 keV isomeric state 3.5 s) and did not have a significant contribution to the fit.

Surrounding the implantation point was the Summing NaI detector (SuN) [52]. SuN is a cylindrical NaI(Tl) scintillator, 16 inches in height and 16 inches in diameter, with a 1.7 inch borehole along its axis. SuN is segmented into eight, optically isolated segments, four above and four below the beam axis. The DSSD implantation detector was placed inside the borehole at the geometric center of SuN. For γ rays emitted at the center of SuN the angular coverage is approximately 98% and the efficiency for single 1 MeV γ full-energy detection is

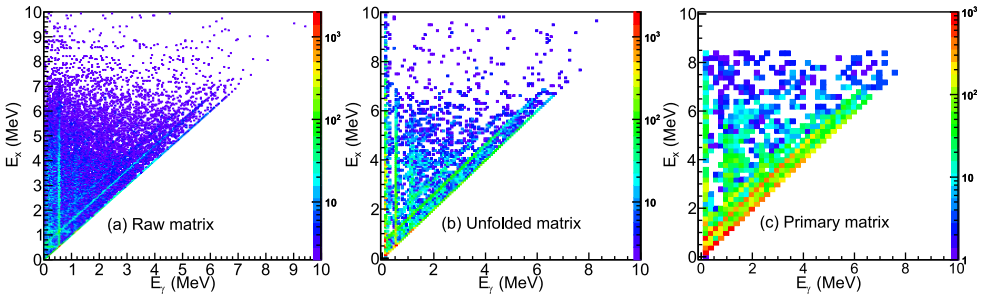

Figure 3. Experimental matrices for ^{69}Ni. (a) Raw matrix (bin = 40 keV), (b) unfolded matrix (bin = 80 keV), (c) primary γ-ray matrix (bin = 200 keV). See text for details.

≈85%. Details about SuN's characterization can be found in [52]. The application of the β-Oslo technique using the SuN detector was presented in two previous publications of our group [27, 29], therefore only a short description of the method will be presented here.

The β-Oslo method relies on the population of the compound nucleus of interest using β decay. Two main pieces of experimental information are required, namely, the populated excitation energy, E_x, and the γ-ray energy, E_γ. E_x can be extracted from SuN by summing all γ-ray energies in an event, following the principle of the technique of total absorption spectroscopy. The segmentation of SuN provides the individual γ-ray energy information, E_γ, by treating each segment as an individual detector. Figure 3(a) shows the raw $E_x - E_\gamma$ matrix for ^{69}Ni populated in the β decay of ^{69}Co. This matrix was created by requiring that the implanted ion was identified as ^{69}Co, a β particle was detected in the same pixel of the DSSD within 800 ms of the ion implantation, and no signal was recorded in the Si veto detector. In addition, random correlation background was also subtracted. It is worth mentioning that the experimental matrix shows significant population at excitation energies above the neutron separation energy ($S_n(^{69}\text{Ni}) = 4.5$ MeV). This effect was also observed in the decay of the neighboring nucleus ^{70}Co [53], and will be explored in more detail for the case of ^{69}Co in a future publication.

Starting with the raw matrix, the β-Oslo method follows four main steps:

- Unfolding of the γ spectra for each initial excitation energy [54].
- Isolation of the primary γ-ray spectrum, i.e., the distribution of the first emitted γ rays in all the γ-decay cascades for each initial excitation energy [25].
- Extraction of the functional form of the NLD and the γ-ray transmission coefficient from the primary γ-ray spectrum [26].
- Normalization of the NLD and γSF [26, 55, 56].

3. Results and discussion

In the present work, the unfolding was done based on the response function of the SuN detector. The response function was created using the GEANT4 simulation package [57, 58], which included a detailed description of the experimental setup, and which was validated in detail against experimental data from various radioactive sources and known resonances. The result of the unfolding procedure is shown in figure 3(b). For the second step, the well developed and characterized method of [25] was used to extract the primary γ-ray distribution per excitation energy. This so called 'first generation' matrix is shown in figure 3(c). The

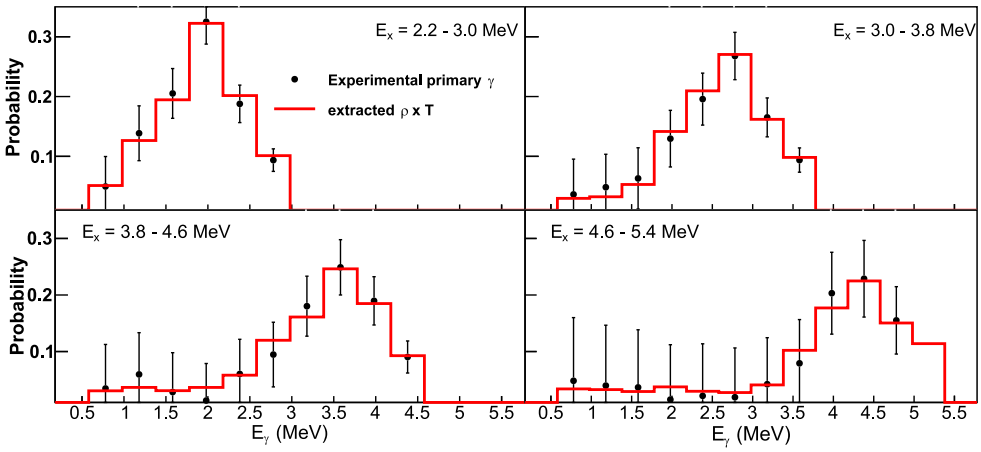

Figure 4. ^{69}Ni primary γ ray distribution. The black dots present the experimental results while the solid/red line shows the extracted $\rho(E_x - E_\gamma) \cdot \mathscr{T}(E_\gamma)$ using the β-Oslo technique.

primary γ-ray spectrum corresponds to the relative probability of a decay with γ-ray energy E_γ from an initial excitation energy E_x, and depends on the NLD at the final excitation energy $\rho(E_x - E_\gamma)$, and the γ-ray transmission coefficient $\mathscr{T}(E_\gamma)$ [26]:

$$P(E_\gamma, E_x) \propto \rho(E_x - E_\gamma) \cdot \mathscr{T}(E_\gamma), \tag{1}$$

where $P(E_\gamma, E_x)$ is the experimental primary γ-ray matrix. Using equation (1), an iterative extraction procedure [26] was applied to obtain the NLD and γSF, from the data within $E_{\gamma,\min} = 1.0$ MeV, and $E_x \in [2.2, 5.4]$ MeV. Therefore, the third step results in the extraction of the functional form of the NLD and the γSF ($f(E_\gamma)$), where for dipole transitions the latter quantity is connected to the $\mathscr{T}(E_\gamma)$ through:

$$f(E_\gamma) = \frac{\mathscr{T}(E_\gamma)}{2\pi E_\gamma^3}. \tag{2}$$

Figure 4 shows a comparison between the experimental primary γ-ray distribution coming from different energy bins (dots), and the extracted $\rho(E_x - E_\gamma) \cdot \mathscr{T}(E_\gamma)$ (red, solid line). The excellent agreement observed in figure 4 shows that the extraction technique works well and the functional form of the ρ and $\mathscr{T}$ can reproduce the experimental data. The error bars shown in the figure come from the statistical uncertainties and also uncertainties introduced during the unfolding and the primary γ ray extraction methods [26].

The fourth step in the analysis procedure is the normalization of the extracted NLD and γSF to known quantities. The NLD was normalized to the experimental level density of the low-lying discrete levels of ^{69}Ni, and the level density at the neutron-separation energy, $\rho(S_n)$. The low-lying level scheme was taken from ENSDF [51] and was assumed to be complete up to 2.5 MeV. No experimental value for neutron resonance spacings (D_0) exists for the nucleus of interest, therefore the $\rho(S_n)$ had to be extracted from theoretical models with a resulting larger systematic uncertainty. Using the tabulated NLD from [40], an energy shift was applied, as described in the original publication, to match the low-lying level scheme. The energy shift upper and lower limit values were -0.4 and -0.8 MeV, respectively. The middle value used a shift of -0.6 MeV. Using these shifts, the upper, middle and lower values for $\rho(S_n)$ were 140, 110, and 90 MeV^{-1}, respectively, and these were used as limits in the

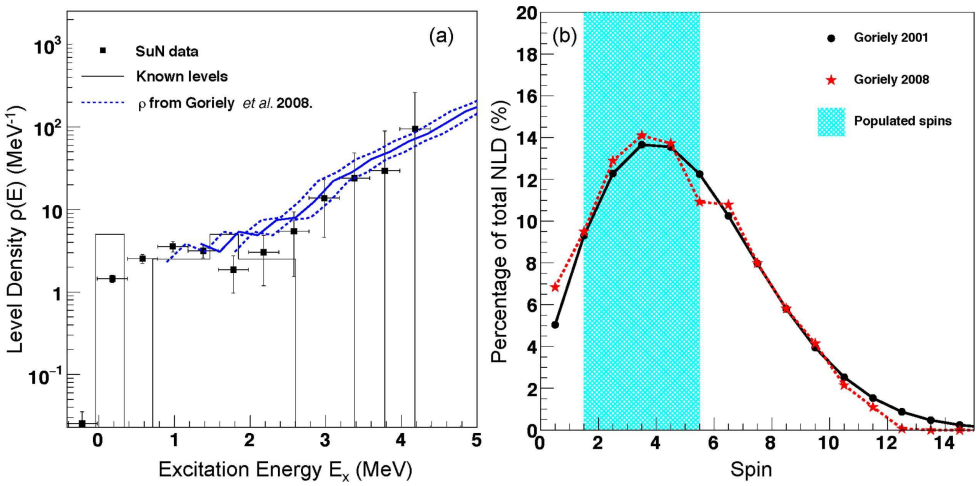

Figure 5. (a) Extracted NLD for ^{69}Ni (black dots). The low-lying levels from ENSDF [51] are shown in the solid black line. The upper and lower limits for the NLD used in the TALYS calculations for the extraction of the ^{68}Ni(n, γ)^{69}Ni reaction cross section are represented by the dashed blue lines, with the middle value indicated by the solid blue line. (b) The ^{69}Ni spin distribution around the neutron separation energy as calculated by [39, 40]. The shaded area shows the part of the distribution that is expected to be populated in the present experiment.

normalization procedure. For consistency, the same model and energy shifts were used for extracting the D_0 values, 37, 39 and 41 keV, respectively. In addition, other NLD models were investigated, such as the Goriely *et al* tabulated level densities [39], which resulted in a $\rho(S_n)$ of 98 MeV^{-1}, and also the Generalized super fluid model (GSM) [37, 38], which gave a $\rho(S_n)$ of 140 MeV^{-1}, following the procedure described above to match the low-lying discrete levels. The results of both NLD models are within the upper and lower limits mentioned above. These limits are shown in figure 5(a) together with the low-lying discrete levels and the experimental data. The experimental data are in good agreement with the discrete levels at low energies, however, the high energies present significant statistical fluctuations. Nevertheless, this experimental result is still useful for constraining the γSF as described below.

The selective spin population of β decay was taken into account in the normalization process. Starting with the $7/2^-$ ground state of ^{69}Co, the allowed transitions will populate $5/2^-$, $7/2^-$ and $9/2^-$ states. The β-Oslo analysis considers the NLD after the emission of one γ ray, and therefore, the populated spin distribution, assuming dominant dipole transitions [41], is expected to be from $3/2$ to $11/2$, of both parities. Using the theoretical spin distribution of [39] and of [40], the above spin range corresponds to 60(5)% of the total, as shown in figure 5(b). This fraction was taken into account in the present analysis. An additional uncertainty comes from the fact that the populated ^{69}Ni has an isomeric state at 321 keV, which β-decays with a half-life of 3.5 s [51]. The presence of this state introduces an uncertainty in the experimentally extracted excitation energy. For this reason, a new upper limit for the NLD was calculated assuming the extreme where the extracted excitation energy is off by the excitation energy of the isomeric state. This assumption is an extreme upper limit for the NLD, however, since it is unknown what fraction of the excitation energy comes from

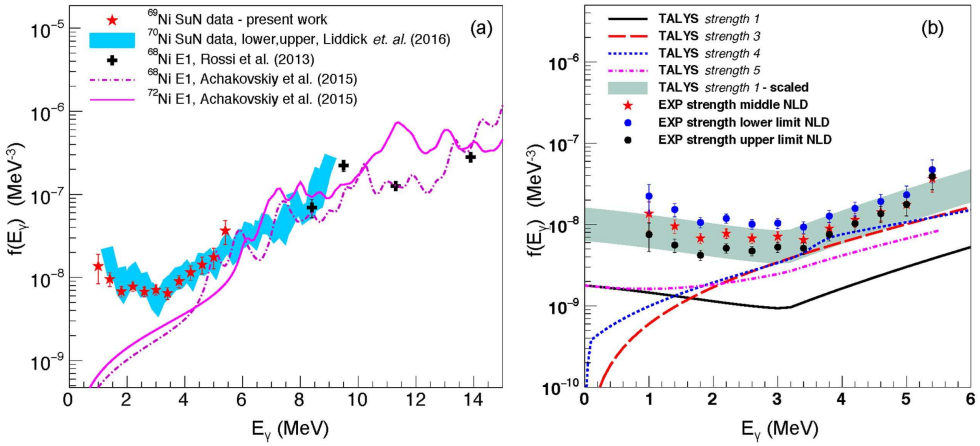

Figure 6. ^{69}Ni γ-ray strength function. (a) The central values from the present work (stars) are compared to recent experimental [29, 59] and theoretical [60] results. (b) The experimental results (central values and upper/lower limits) are compared to the theoretical models from the TALYS package, as presented in table 1. The shaded area shows the upper and lower limits of the γSF that was used as input in the TALYS calculations.

the ground state, and what fraction comes from the isomeric state, the full uncertainty was included in the analysis. This new upper limit for $\rho(S_n)$ was 225 MeV^{-1}.

On top of the NLD normalizations, the γSF was also normalized using available experimental data. In the traditional Oslo method, this normalization is done using the average radiative width of levels near the neutron separation energy, $\langle\Gamma_\gamma\rangle$. Since in the case of ^{69}Ni the Γ_γ is not known, the normalization was done using existing experimental data in the nickel isotopic chain. These include the Coulomb dissociation of ^{68}Ni [59] and the γSF of ^{70}Ni as extracted previously using the β-Oslo method [29]. The results are shown in figure 6(a). While the absolute scaling is a result of the aforementioned normalization, it can be observed that the shape of the distribution is in excellent agreement with the previous measurements. Figure 6(b), shows the experimental middle values (stars), as well as the upper and lower limits of the γSF, as extracted using the aforementioned upper and lower limits of the NLD. These are compared to the four γSF models from the TALYS package that are included in table 1. It can be observed that the Kopecky–Uhl generalized Lorentzian model (*strength 1*) [41] reproduces the shape of the experimental data very well. For this reason, this model was scaled up by a factor of 3.5 to represent the lower limit of the experimental data and by a factor of 9 to represent the upper limit of the experimental data (shaded area). It can be observed that while the other three models presented in the figure are in fair agreement with the data above $\approx$3 MeV, large discrepancies are observed at low energies. In addition, it should be noted that for simplicity, the default scaling of the γSF in the TALYS code (parameter *gnorm*) was set to 1 for the comparison in figure 6(b). The extracted NLD and γSF are presented in tables 2 and 3.

Using the extracted NLD and γSF for ^{69}Ni, as well as the upper and lower limits, the cross section and reaction rate of the ^{68}Ni(n, γ)^{69}Ni were calculated. These are shown in figures 7(a) and (b), respectively. In both panels, the dark, shaded area represents the upper/lower limits of the present work, while the middle value is shown in the black, solid line. The blue, dashed line presents theoretical calculations using the code Non-Smoker [63]

Table 2. Extracted nuclear level density and γ-ray strength function as shown in figures 5(a) and 6(b).

E_x	$\rho(E_x)$ (MeV^{-1})			E_γ	$f(E_\gamma)$ 10^{-8} (MeV^{-3})		
(MeV)	Middle	Upper	Lower	(MeV)	Middle	Upper	Lower
0.2	1.6	1.3	1.6	1	1.4	3.1	0.5
0.6	2.6	2.4	2.7	1.4	1.0	1.8	0.5
1.0	3.6	3.5	3.6	1.8	0.7	1.2	0.4
1.4	3.1	3.2	3.0	2.2	0.8	1.3	0.4
1.8	1.8	1.9	1.7	2.6	0.7	1.1	0.4
2.2	2.8	3.3	2.6	3	0.7	1.2	0.5
2.6	4.8	6.0	4.5	3.4	0.6	1.1	0.4
3.0	11.9	15.8	10.7	3.8	0.9	1.5	0.6
3.4	20.0	28.3	17.7	4.2	1.2	1.9	0.8
3.8	23.9	36.1	20.6	4.6	1.4	2.4	1.0
4.2	74.8	120.0	63.0	5	1.8	3.0	1.3
4.6	187.6	320.5	154.6	5.4	3.7	6.2	2.7
5.0	169.6	278.2	139.7				

Table 3. Astrophysical reaction rate extracted in the present work. The first and fifth columns correspond to the temperature in GK. The values for the middle, upper, and lower limits as shown in figure 7(b), are shown in the remaining columns.

T	Rate 10^5 (cm^{-3} s^{-1} mol^{-1})			T	Rate 10^5 (cm^{-3} s^{-1} mol^{-1})		
(GK)	Middle	Upper	Lower	(GK)	Middle	Upper	Lower
0.0001	7.00	12.88	4.52	0.80	1.06	1.92	0.67
0.0005	4.24	7.51	2.85	0.90	1.06	1.93	0.67
0.001	3.41	5.88	2.33	1.00	1.07	1.94	0.67
0.005	2.44	4.11	1.68	1.50	1.15	2.10	0.72
0.01	2.06	3.51	1.41	2.00	1.29	2.35	0.79
0.05	1.52	2.63	1.02	2.50	1.47	2.70	0.89
0.1	1.38	2.41	0.91	3.00	1.70	3.14	1.01
0.15	1.30	2.29	0.84	3.50	1.99	3.70	1.17
0.2	1.24	2.21	0.80	4.00	2.36	4.44	1.36
0.25	1.20	2.14	0.77	5.00	3.44	6.67	1.87
0.3	1.16	2.09	0.74	6.00	4.91	9.87	2.52
0.4	1.12	2.02	0.71	7.00	6.03	12.52	2.94
0.5	1.09	1.97	0.69	8.00	5.72	12.16	2.68
0.6	1.07	1.94	0.68	9.00	4.36	9.44	1.98
0.7	1.06	1.93	0.67	10.00	3.02	6.63	1.34

(figure 7(a)), which also corresponds to the JINA-REACLIB results [61] (figure 7(b)). The dotted–dashed line shows the recommended rate of the reaction library BRUSLIB [62]. The light shaded area shows the upper and lower limits of default TALYS calculations using the different models for NLD and γSF listed in table 1. Both reaction libraries used in astrophysical calculations, JINA-REACLIB and BRUSLIB, are in good agreement with the

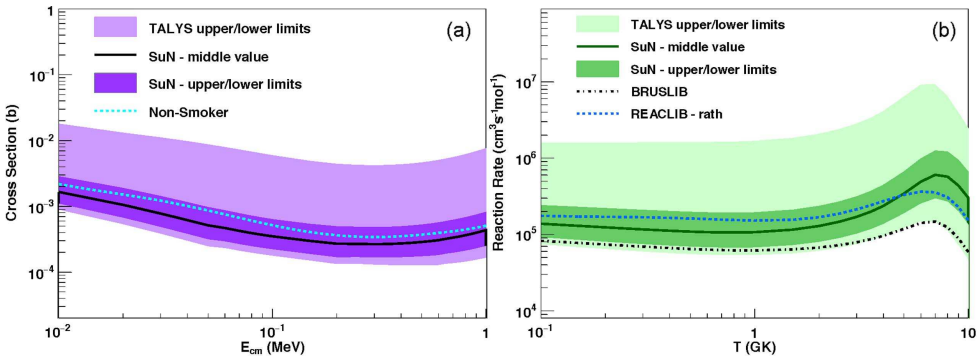

Figure 7. ^{68}Ni(n, γ)^{69}Ni cross section (a) and reaction rate (b). The light shaded bands correspond to TALYS calculations using default NLD and γSF models as described in table 1. The darker shaded bands correspond to the results of the present work. Calculations using the Non-Smoker code, which are also used in the JINA REACLIB [61] are shown in the dotted line. The dashed–dotted line represents the reaction library BRUSLIB [62].

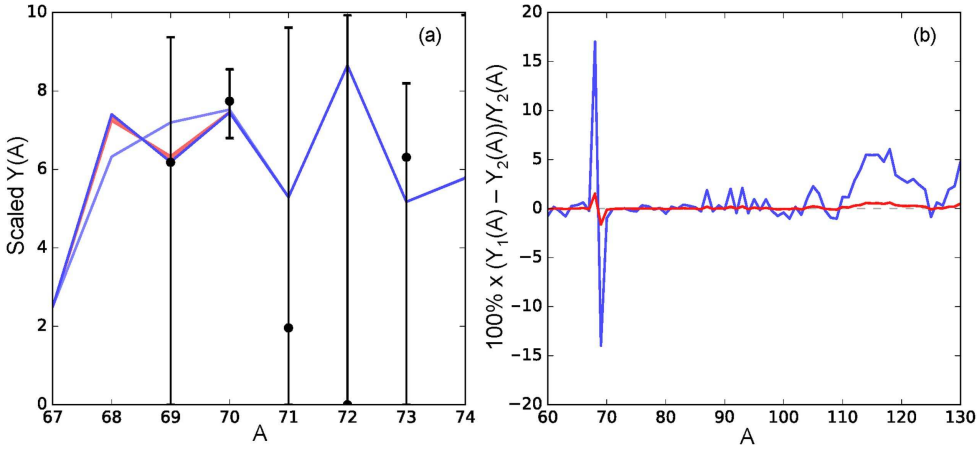

Figure 8. (a) Calculated abundance distribution as a function of mass number for the weak r process, compared to solar r-process residuals (black dots) [5]. The abundance patterns are compared using JINA REACLIB rates with a variation in the ^{68}Ni(n, γ)^{69}Ni reaction rate of one order of magnitude (blue), and the experimentally constrained reaction rate from the present work (red, shaded area). (b) Comparison of the percent abundance change as a function of mass number using old reaction rate uncertainties (blue line) versus the present experimentally constrained reaction rate (red). The present data reduce the uncertainties in the abundance predictions to less than 2.5% across the mass range.

extracted experimental reaction rates, with the JINA-REACLIB recommended rate overlapping with the experimental range, and the BRUSLIB rate being slightly lower than the lower limit. The uncertainty associated with the extracted rate is around a factor of 3 (from lower to upper limits). While the statistics of the experiment were limited, the main source of uncertainty is associated with the normalization process. The fact that no level spacing parameters are known for ^{69}Ni leads to the use of a wide range of level density normalization

values that rely on theoretical calculations. Nevertheless, even with the larger systematic uncertainty, the extracted reaction rate provides a significant constraint for the ^{68}Ni(n, γ)^{69}Ni reaction.

The impact of the neutron optical model potential on the present result was also investigated. For this, the two available nOMP models in TALYS were used, namely the semi-microscopic OMP of Jeukenne–Lejeune–Mahaux [64], and the phenomenological model of Koning and Delaroche [65]. The cross sections calculated with the two OMP models were different at most by 10%, well within the uncertainties of the present result.

The experimentally constrained reaction rate of the ^{68}Ni(n, γ)^{69}Ni reaction was used in astrophysical calculations for low entropy r-process scenarios that mainly produce the $A \approx 80$ peak (weak r process). Such scenarios are the accretion disk outflows that accompany a neutron star [13] or black hole–neutron star merger [66]. The weak r-process parametrization was done with the following wind conditions: entropy $s/k = 10$, time scale $= 0.1$ s, and electron fraction $Y_e = 0.32$, similar to [13, 66]. The results of these weak r-process calculations are shown in figure 8. The black dots in figure 8(a) correspond to solar r-process residuals taken from [5]. The blue lines represent the calculated abundances when varying the rate of the ^{68}Ni(n, γ)^{69}Ni reaction within its theoretical deviations, while the narrow, red, shaded area shows the impact of the experimental results. Figure 8(b) shows the same calculations in the form of a ratio between the upper and lower limits. Both figures show that this particular rate has a local impact in the $A \approx 67$–70 mass region and a smaller global impact, especially around $A = 120$. The uncertainty associated with this reaction is significantly reduced by the present result and is now well within the observation uncertainties for mass 70 nuclei.

4. Conclusions

The cross section and reaction rate of the ^{68}Ni(n, γ)^{69}Ni reaction have been experimentally constrained for the first time. The β-Oslo method was used for extracting the NLD and the γ-ray strength function of ^{69}Ni, which was populated in the β decay of ^{69}Co. This measurement provided the first experimental information on these two quantities for ^{69}Ni, and they were used as input in statistical model calculations for constraining the ^{68}Ni(n, γ)^{69}Ni reaction. The various sources of systematic uncertainty were investigated, and the final uncertainty on the reaction rate was reduced to a factor of $\approx$3. This is a significant reduction compared to the theoretical deviations of a factor 35 at 1.5 GK. The present result reduces the uncertainties in the abundance predictions from the ^{68}Ni(n, γ)^{69}Ni reaction to less than 2.5% across the mass range $A = 67$–70. In addition, the half-life of ^{69}Co was measured to be 216(15) ms, in excellent agreement with the literature.

Acknowledgments

We gratefully acknowledge the support of NSCL operations staff. Financial support from the Research Council of Norway, project grant no. 205528 (ACL and MG) and project grant no. 210007 (LCC, TR and SS) is gratefully acknowledged. ACL acknowledges funding through the ERC-STG-2014 under grant agreement no. 637686. DLB acknowledges the support of LLNL under Contract DE-AC52-07NA27344. The LANL work was carried out under the auspices of the NNSA of the US Department of Energy at Los Alamos National Laboratory under Contract No. DE-AC52-06NA25396. This work was supported by the National Science Foundation under Grants No. PHY 1102511 (NSCL) and No. PHY 1430152 (Joint Institute

for Nuclear Astrophysics), and PHY 1350234 (CAREER). This material is based upon work supported by the Department of Energy/National Nuclear Security Administration under Award Numbers DE-NA0003221, DE-NA-0000979 and DE-NA-0002132.

References

[1] Burbidge K M, Burbidge G R, Fowler W A and Hoyle F 1957 *Rev. Mod. Phys.* **29** 547
[2] Cameron A G W 1957 *Pub. Astron. Soc. Pac.* **69** 201
[3] Abbott B *et al* 2016 *Phys. Rev. Lett.* **116** 061102
[4] Käppeler F, Gallino R, Bisterzo S and Aoki W 2011 *Rev. Mod. Phys.* **83** 157
[5] Arnould M, Goriely S and Takahashi K 2007 *Phys. Rep.* **450** 97
[6] Sneden C, Cowan J J and Gallino R 2008 *Annu. Rev. Astron. Astrophys.* **46** 241
[7] Arnould M and Goriely S 2003 *Phys. Rep.* **384** 1
[8] Rauscher T, Dauphas N, Dillmann I, Fröhlich C, Fülöp Z and Gyürgy G 2013 *Rep. Prog. Phys.* **76** 066201
[9] Woosley S, Wilson J, Mathews G, Hoffman R and Meyer B 1994 *Astroph. J.* **433** 229
[10] Hüdepohl L, Müller B, Janka H-T, Marek A and Raffelt G 2010 *Phys. Rev. Lett.* **104** 251101
[11] Fischer T, Whitehouse S, Mezzacappa A, Thielemann F-K and Liebendörfer M 2010 *Astron. Astroph.* **517** A80
[12] Martínez-Pinedo G, Fischer T, Lohs A and Huther L 2012 *Phys. Rev. Lett.* **109** 251104
[13] Wanajo S, Sekiguchi Y, Nishimura N, Kiuchi K, Kyutoku K and Shibata M 2014 *Astroph. J.* **789** L39
[14] Just O, Bauswein A, Pulpillo R, Goriely S and Janka H-T 2015 *Mon. Not. R. Astron. Soc.* **448** 541
[15] Mendoza-Temis J D J, Wu M-R, Langanke K, Martínez-Pinedo G, Bauswein A and Janka H-T 2015 *Phys. Rev.* C **92** 055805
[16] Metzger B D, Martínez-Pinedo G, Darbha S, Quataert E, Arcones A, Kasen D, Thomas R, Nugent P, Panov I V and Zinner N T 2010 *Mon. Not. R. Astron. Soc.* **406** 2650
[17] Ji A, Frebel A, Chiti A and Simon J 2016 *Nature* **531** 610
[18] Surman R, Mumpower M, Sinclair R, Jones K L, Hix W R and McLaughlin G C 2014 *AIP Adv.* **4** 041008
[19] Mumpower M, Surman R, McLaughling G C and Aprahamian A 2016 *Prog. Part. Nucl. Phys.* **86** 86
[20] Martin D, Arcones A, Nazarewicz W and Olsen E 2016 *Phys. Rev. Lett.* **116** 121101
[21] Forssen C, Dietrich F, Escher J, Hoffman R and Kelley K 2007 *Phys. Rev.* C **75** 055807
[22] Cizewski J, Hatarik R, Jones K, Pain S, Thomas J, Johnson M, Bardayan D, Blackmon J, Smith M and Kozub R 2007 *Nucl. Instrum. Methods* B **261** 938
[23] Escher J E, Burke J T, Dietrich F S, Scielzo I J T N D and Younes W 2012 *Rev. Mod. Phys.* **84** 353
[24] Utsunomiya H *et al* 2010 *Phys. Rev.* C **82** 064610
[25] Guttormsen M, Ramsøy T and Rekstad J 1987 *Nucl. Instrum. Methods* A **255** 518
[26] Schiller A, Bergholt L, Guttormsen M, Melby E, Rekstad J and Siem S 2000 *Nucl. Instrum. Methods* A **447** 498
[27] Spyrou A *et al* 2014 *Phys. Rev. Lett.* **113** 232502
[28] Wang M, Audi G, Wapstra A, Kondev F, MacCormick M, Xu X and Pfeiffer B 2012 *Chin. Phys.* C **36** 1603
[29] Liddick S *et al* 2016 *Phys. Rev. Lett.* **116** 242502
[30] Koning A, Hilaire S and Duijvestijn M C 2008 *TALYS-1.6: Proc. Int. Conf. on Nuclear Data for Science and Technology ND2004 (Nice, France, April 22–27, 2007)* pp 211–4
[31] Goriely S and Delaroche J-P 2007 *Phys. Lett.* B **653** 178
[32] Hilaire S, Girod M, Goriely S and Koning A J 2012 *Phys. Rev.* C **86** 064317
[33] Brink D 1957 *Nucl. Phys.* **4** 215
[34] Axel P 1962 *Phys. Rev.* **126** 671
[35] Dilg W, Schantl W, Vonach H and Uhl M 1973 *Nucl. Phys.* A **217** 269
[36] Gilbert A and Cameron A G W 1965 *Can. J. Phys.* **43** 1446
[37] Ignatyuk A, Istekov K and Smirenkin G 1979 *Sov. J. Nucl. Phys.* **29** 450
[38] Ignatyuk A V, Weil J L, Raman S and Kahane S 1993 *Phys. Rev.* C **47** 1504
[39] Goriely S, Tondeur F and Pearson J 2001 *At. Data Nucl. Data Tables* **77** 311
[40] Goriely S, Hilaire S and Koning A 2008 *Phys. Rev.* C **78** 064307

[41] Kopecky J and Uh M 1990 *Phys. Rev.* C **41** 1941
[42] Goriely S and Khan E 2002 *Nucl. Phys.* A **706** 217
[43] Goriely S, Khan E and Samyn M 2004 *Nucl. Phys.* A **739** 331
[44] Goriely S 1998 *Phys. Lett.* B **436** 10
[45] Morrissey D J, Sherrill B, Steiner M, Stolz A and Wiedenhoever I 2003 *Nucl. Instrum. Methods* B **204** 90
[46] Bernas M, Armbruster P, Czajkowski S, Faust H, Bocquet J P and Brissot R 1991 *Phys. Rev. Lett.* **67** 3661
[47] Mueller W F *et al* 1999 *Phys. Rev. Lett.* **83** 3613
[48] Sorlin O *et al* 1999 *Nucl. Phys.* A **660** 3
[49] Gaudefroy L 2005 Etude de la fermeture de couches $N = 28$: implication astrophysique. Spectroscopie Béta Gamma de noyaux riches en neutrons *Physique Nucléaire Théorique [nucl-th] (Université Paris Sud—Paris XI)*
[50] Daugas J M *et al* 2011 *Phys. Rev.* C **83** 054312
[51] National Nuclear Data Center 2012 Evaluated Nuclear Structure Data File (ENSDF) Retrieval, www.nndc.bnl.gov
[52] Simon A *et al* 2013 *Nucl. Instrum. Methods* A **703** 16
[53] Spyrou A *et al* 2016 *Phys. Rev. Lett.* **117** 142701
[54] Guttormsen M *et al* 1997 *Nucl. Instrum. Methods* A **374** 371
[55] Voinov A, Guttormsen M, Melby E, Rekstad J, Schiller A and Siem S 2001 *Phys. Rev.* C **63** 044313
[56] Larsen A C *et al* 2011 *Phys. Rev.* C **83** 034315
[57] Agostinelli S *et al* 2003 *Nucl. Instrum. Methods* A **506** 250
[58] Allison J *et al* 2006 *IEEE Trans. Nucl. Sc.* **53** 270
[59] Rossi D M *et al* 2013 *Phys. Rev. Lett.* **111** 242503
[60] Achakovskiy O, Avdeenkov A, Goriely S, Kamerdzhiev S and Krewald S 2015 *Phys. Rev.* C **91** 034620
[61] Cyburt R H *et al* 2010 *Astrophys. J. Suppl.* **189** 240
[62] The Brussels Nuclear Library for Astrophysics Applications, maintained by Institut d'Astronomie et d'Astrophysique, Université Libre de Bruxelles; http://astro.ulb.ac.be/bruslib/
[63] Rauscher T and Thielemann F-K 2000 *At. Data Nucl. Data Tables* **75** 1
[64] Jeukenne J P, Lejeune A and Mahaux C 1977 *Phys. Rev.* C **15** 10
[65] Koning A J and Delaroche J P 2003 *Nucl. Phys.* A **713** 2003
[66] Surman R, McLaughlin G C, Ruffert M, Janka H-T and Hix W R 2008 *Astrophys. J. Lett.* **679** L117